

## Supporting Information

### Cu@TiO<sub>2</sub> Janus microswimmers with versatile motion mechanism

#### Experimental

##### Materials and reagents

Titanium (IV) iso-propoxide (TTIP) was purchased from Alfa Aesar Co. Ltd. Dodecylamine (DDA) was obtained from Fluka. SiO<sub>2</sub> particles were obtained from Sigma Co. Ltd. All other reagents including methanol and acetonitrile were of analytical grade and used as received without further treatment.

##### Synthesis of mesoporous TiO<sub>2</sub>

TiO<sub>2</sub> particles were synthesized via hydrolysis and condensation reaction of TTIP.<sup>1</sup> In brief, 0.18 mL of water was added to mixture solution containing 105 mL of methanol and 45 mL of acetonitrile. Then 0.28 g of DDA was dissolved in the mixture under stirring. After stirring for 10 min, 1 mL of TTIP was added dropwisely and stirred for 12 h. DDA acted as a catalyst and molecular template to introduce the pores into the TiO<sub>2</sub> particles. Then the particles were washed with methanol three times and were dried at 80°C. The particles were heated in tubular furnace under nitrogen flow and air for 2h at 600°C, and then the black and white TiO<sub>2</sub> particles were obtained respectively. The size of both of them is around 700 nm, which can be confirmed by DLS measurements and TEM images (Figure S1a, b and discussion in the SI).

The XRD patterns shown in Figure 1d and Figure S2 display that both white and black TiO<sub>2</sub> particle exhibit an anatase–rutile mixed crystalline phase (assignment of the single peaks is given in the SI). Since we observed very similar behaviors for both, the rest of the manuscript we are focusing on the study of black TiO<sub>2</sub> based light driven micromotors to investigate the motion behaviors and active-passive interactions.

Even though generally anatase is considered more reactive than rutile, the different oxidation mechanism might be more favourable for achieving micromotion, since it is capable of forming a Ti-OO-Ti surface structure that readily forms O<sub>2</sub> (scheme in Figure S3)<sup>2, 3, 4</sup>, which has a lower diffusion constant and therefore creates more pronounced product gradients than H<sub>2</sub> would (see also more detailed explanation in Sx). Furthermore, for the mixed phase rutile-anatase TiO<sub>2</sub>, a large number of oxygen vacancies are present at the surface of TiO<sub>2</sub>, which lower the band gap of defective TiO<sub>2</sub> and act as efficient trap center of electrons. Therefore, they increase the separation of the charge carriers and delay the recombination of electron-hole pairs thus resulting in efficient photocatalytic activity.<sup>5,6</sup> Generally, it is assumed that structural and surface properties affect both, the charge carriers separation step and the reagents adsorption on active sites, leading to significant differences in photochemical activity, but these mechanistic details will be analyzed in further work.

##### Synthesis of Janus Cu@TiO<sub>2</sub> and Au@TiO<sub>2</sub> particles

For the Janus Cu@TiO<sub>2</sub> and Au@TiO<sub>2</sub> particles, 200 μL of the TiO<sub>2</sub> particles suspension was spread onto glass slides and dried to form particle monolayers. Then TiO<sub>2</sub> particles were coated with a copper and gold layer (about 30 nm in thickness) via thermal deposition. Then the Cu@TiO<sub>2</sub> and Au@TiO<sub>2</sub> Janus particles were released from the glass by ultrasonication.

##### Manipulation of Micromotors

The motion of Cu@TiO<sub>2</sub> and Au@TiO<sub>2</sub> micromotors was investigated by an optical microscope (Carl Zeiss Microscopy GmbH, Gemarny) equipped with a Zeiss Colibri lamp. The UV light (385 nm) was used to and study the motion behaviors in water and 0.5% H<sub>2</sub>O<sub>2</sub> solution. The 100% intensity of UV light is 315 mW. For the movement behaviors of micromotors in water and peroxide solution, 50% (157.5 m W) UV light was used. 1.5%, 10%, 20% and 25% UV light are corresponding to 4.725, 31.5, 63 and 78.75 mW, respectively.

##### Active-passive interactions

For the study of interactions between active (Cu@TiO<sub>2</sub> or Au@TiO<sub>2</sub>) and passive particles, 5 μL of active particles, 1 μL of SiO<sub>2</sub> (0.025%, 2 μm) particles, and 6 μL of 1% H<sub>2</sub>O<sub>2</sub> were mixed on the cleaning slide.

Zeta potential values, individual measurements in milliQ water gave the listed values:

	In H <sub>2</sub> O (mV)	In H <sub>2</sub> O <sub>2</sub> (mV)
TiO <sub>2</sub>	-6.42 ±0.38	-31.6 ±0.44
SiO <sub>2</sub>	-38.2 ±0.35	-36.8±0.21

For Cu@TiO<sub>2</sub> the measurements in H<sub>2</sub>O<sub>2</sub> are affected by uncontrolled bubble formation at the electrodes of the measurement cell. Consequently, no reliable Zetapotential data can be provided.

### Theoretical considerations

The self-diffusiophoretic model<sup>7,8</sup> employed is defined as follows: Upon UV illumination, at the surface of the TiO<sub>2</sub> particle there is an outward flux  $k$  of product ("solute") which is proportional to the intensity of light and the peroxide concentration. The solute number density field  $C(\mathbf{r})$  is governed by the Laplace equation,  $D \nabla^2 C(\mathbf{r}) = 0$ , where  $\mathbf{r}$  denotes a point in the liquid solution and  $D$  is the diffusion coefficient of the solute. The boundary conditions on the solute number density field are:  $-D [\mathbf{n} \cdot \nabla C] = k$  over the surface of the particle,  $-D [\mathbf{n} \cdot \nabla C] = 0$  on the wall, and vanishing  $C$  far from the particle (where  $\cdot$  denotes the scalar product and  $\mathbf{n}$  the unit vector normal to the surface).

The suspending fluid is assumed to be an incompressible Newtonian liquid of viscosity  $\eta$ , and we assume small Reynolds number  $Re$ ; the hydrodynamic flow  $\mathbf{u}(\mathbf{r})$  and the pressure  $P(\mathbf{r})$  thus are governed by the Stokes equation  $-\nabla P + \eta \nabla^2 \mathbf{u} = 0$  and the incompressibility condition  $\nabla \cdot \mathbf{u} = 0$ . The excess interaction of the solute molecules with the particle surface drives a surface flow that is modeled by an effective slip velocity (phoretic slip)  $\mathbf{v}_s(\mathbf{r}_s) = -b \nabla_{||} C(\mathbf{r}_s)$ , with  $\mathbf{r}_s$  denoting a point on the surface of the particle and  $\nabla_{||}$  the projection of the gradient onto the tangent plane of the surface. The factor  $b$  is a material dependent parameter (the so-called "phoretic" mobility) that encapsulates the molecular details of the interaction between the solute and the surface;  $b < 0$  corresponds to a repulsive interaction, and  $b > 0$  to an attractive one. Thus, the flow  $\mathbf{u}(\mathbf{r})$  obeys the boundary conditions  $\mathbf{u}(\mathbf{r} = \mathbf{r}_s) = \mathbf{U} + \mathbf{\Omega} \times (\mathbf{r}_s - \mathbf{r}_p) + \mathbf{v}_s(\mathbf{r}_s)$  on the particle surface, where  $\mathbf{r}_p$  denotes the position vector of the center of the particle, while  $\mathbf{U}$  and  $\mathbf{\Omega}$  are the (yet unknown) translational and angular velocities of the particle, respectively. The other boundary conditions for the flow are: no slip at the wall, i.e.,  $\mathbf{u}(\mathbf{r} \text{ at the wall}) = 0$  on the wall, and vanishing value (quiescent fluid) far from the particle. The system of equations is closed by the force and torque balance equation, i.e., requiring that the external forces and torques acting on the particle are exactly equal and opposite to the hydrodynamic force and torque exerted by the flow on the particle.

For the case of the spherical, uniformly active particle of radius  $R$  above a planar wall, due to the cylindrical symmetry the only possible motion is translation along the normal (the  $z$ -direction) to the plane, i.e.,  $\mathbf{\Omega} = 0$  and the translational velocity has only one component,  $U_z$ . The external forces acting on the particle are the apparent (buoyancy compensated) weight and the wall-particle surface interactions (electrostatic double layer, van der Waals, etc.); the height  $H$  above the surface, at which the particle "floats",  $U_z = 0$ , is thus determined by the solution of the above two boundary problems with vanishing  $\mathbf{U}$  and  $\mathbf{\Omega}$  and obeying the force balance at that height. For illustration purposes, here we chose the parameters (mass density of particle, surface interactions) such that  $H = R/10$  (i.e., for a micron-sized particle, the corresponding  $H$  is of the order of 100 nm). Both boundary value problems (i.e., for the number density of the solute and for the hydrodynamic flow) can be solved exactly in terms of series representations in bi-polar coordinates; here we simply adapt and employ the solutions available in Ref. <sup>9</sup>.

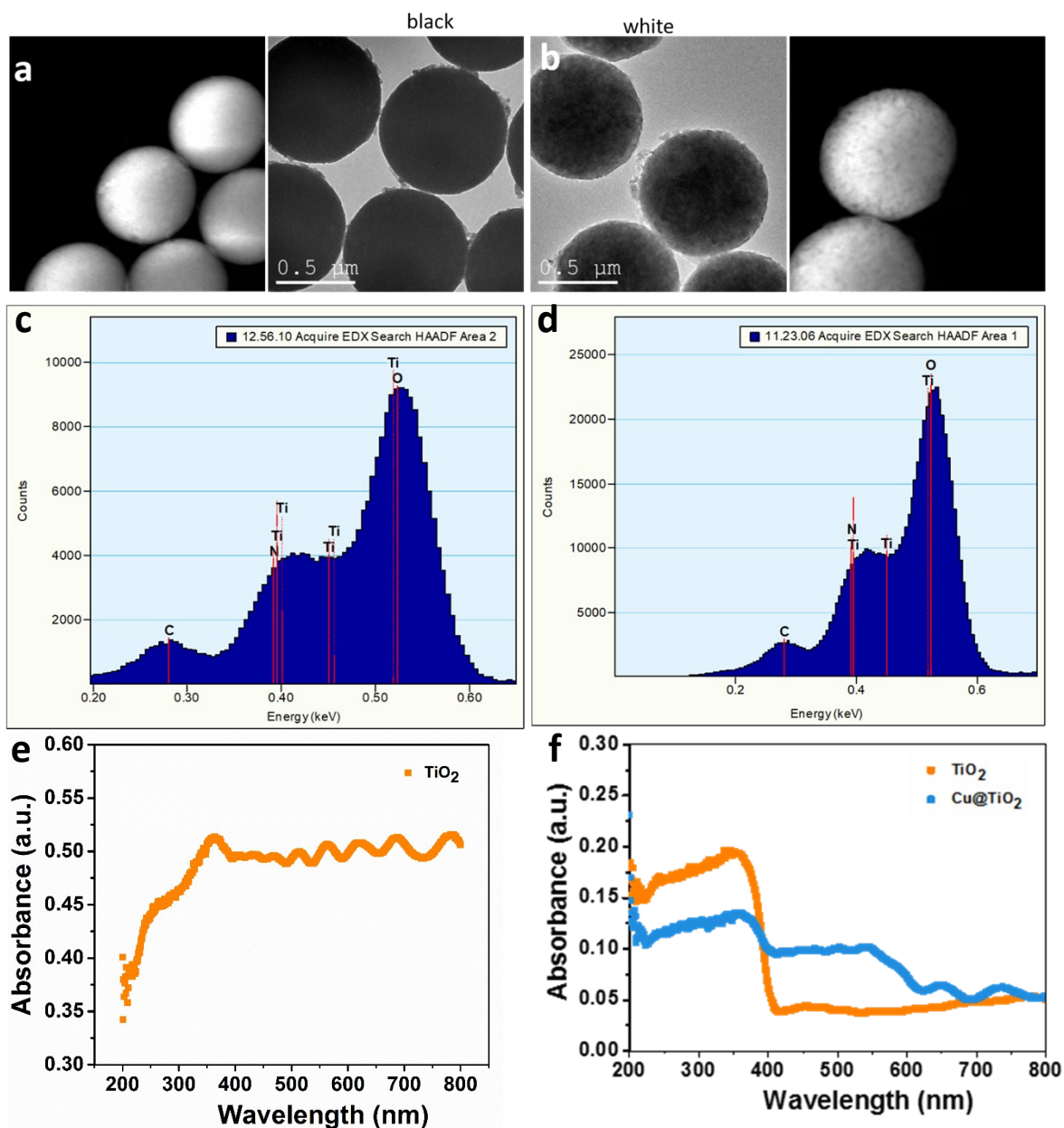


**Fig. S1** TEM, EDX and UV-vis diffuse reflectance spectra of black (a, c, e) and white TiO<sub>2</sub> (b, d, f) particles

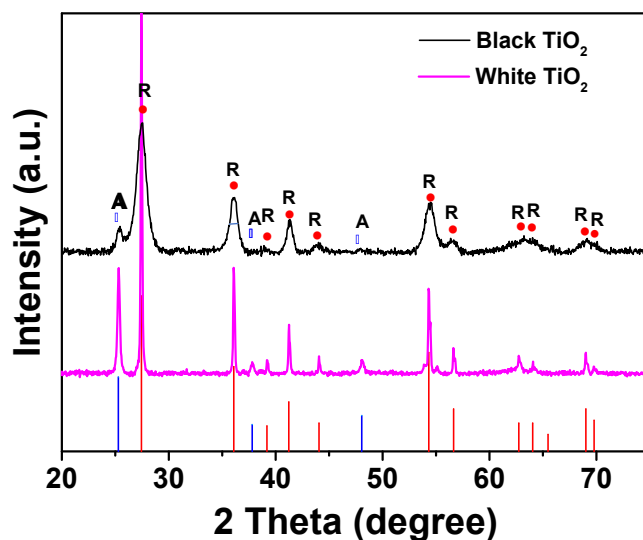


Fig. S2 XRD patterns of black and white TiO<sub>2</sub> particles

Evaluation of XRD: The diffraction peaks located at  $2\theta=27.4^\circ$ ,  $36.0^\circ$ ,  $41.0^\circ$ ,  $44.0^\circ$ ,  $54.0^\circ$ ,  $56.0^\circ$ ,  $62.7^\circ$  and  $69.0^\circ$  correspond to (110), (101), (111), (210), (211), (220), (002) and (301) planes for rutile TiO<sub>2</sub> (PDF No. 21-1276), while the diffraction peaks at  $2\theta=25.2^\circ$  and  $48.0^\circ$  correspond to the (101) and (200) planes for anatase TiO<sub>2</sub> (PDF No.21-1272).

Calculation of the domain sizes using the Debye Scherer equation:

$$B = k \cdot \lambda / S \cdot \cos\theta$$

B.... half width of the peak

k ...constant for spherical particles =0.89

$\theta$ ...diffr. Angle = $36.1^\circ$

$\lambda$  ...wave length (XRD radiation) =0.154 nm

S... domain size

The B values for black TiO<sub>2</sub> and white TiO<sub>2</sub> were determined as 0.9 and 0.2 degrees, which leads to domain sizes of about 9 nm and 40 nm, respectively. These values are to be used only as an estimate, since the XRD has a geometry based broadening of the peaks.

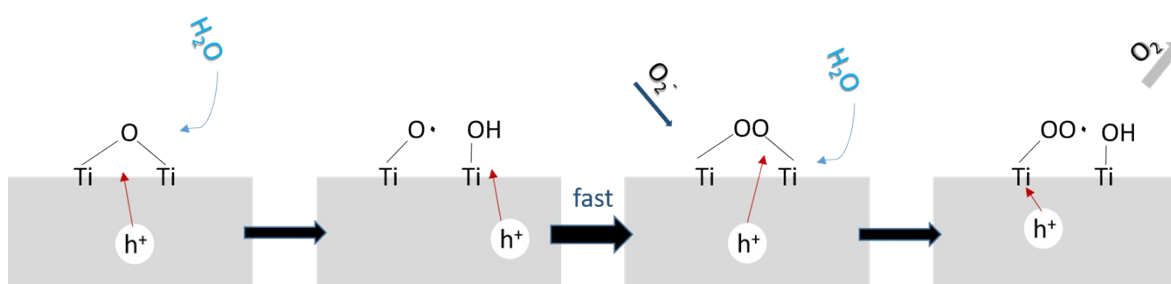


**Fig. S3** Mechanism of O<sub>2</sub> formation on rutile surfaces: Since the Ti–Ti distance on a rutile surface is smaller than for anatase, rutile is capable of forming Ti–OO–Ti surface structures, (analogously to absorbed H<sub>2</sub>O<sub>2</sub>), leading to readily form O<sub>2</sub> by further oxidation, in analogy to.<sup>3</sup>

Since the two molecules have quite different sizes and molecular weights, also their diffusion constants differ (according to Stokes Einstein  $D = k_B T / (6\pi\eta R)$  with  $R$  being the hydrodynamic radius,  $\eta$  the viscosity). The diffusion constant decides the timescale of the establishing the steady-state profiles and all the density profiles of products and gradients depend on these profiles which increase with larger  $D$  values, leading to stronger gradients and more propulsion force.

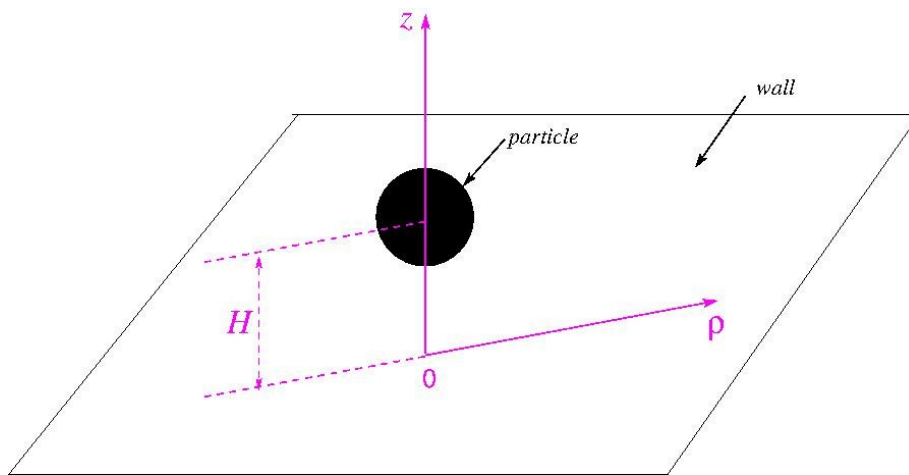


**Fig. S4.** Schematic diagram of the setup for the model calculations.

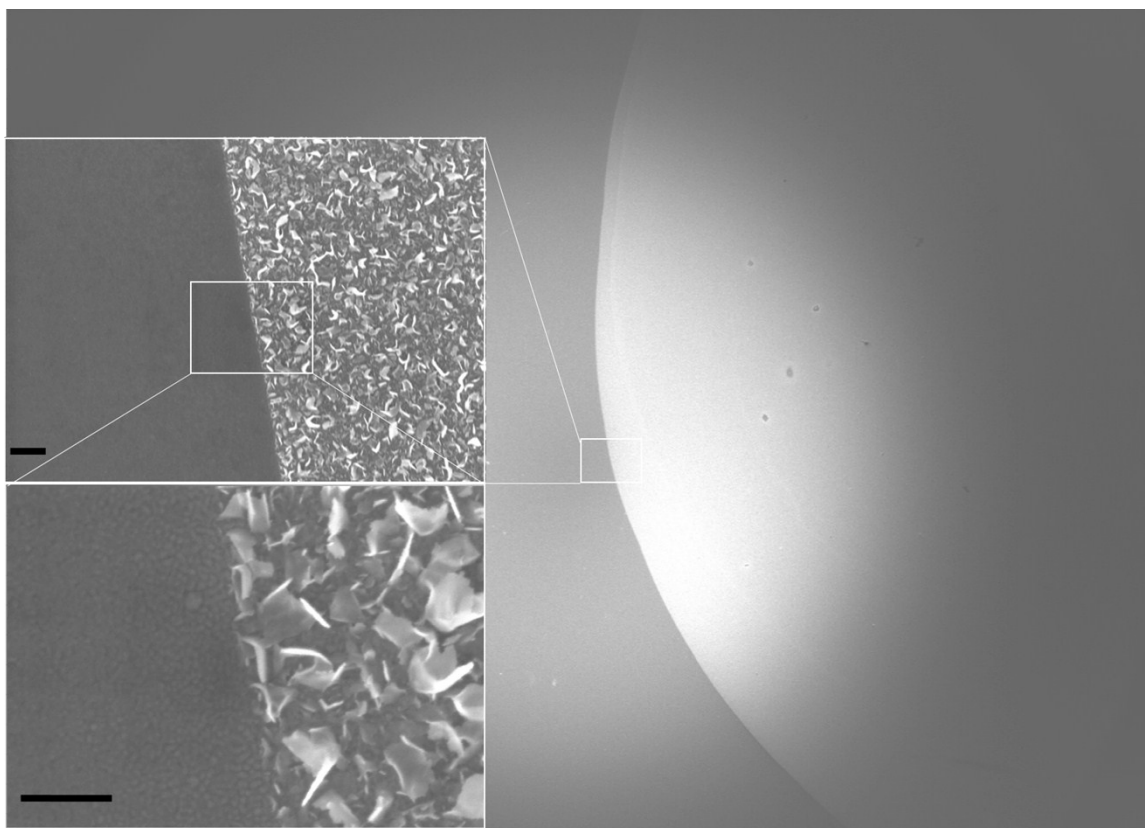


**Fig. S5** SEM micrograph of a deposited Cu film after exposure to one drop of 1%  $\text{H}_2\text{O}_2$ . The oxidized areas appear lighter due to surface irregularities, which seem like flakes in the magnifications. Scale bar, 200nm.

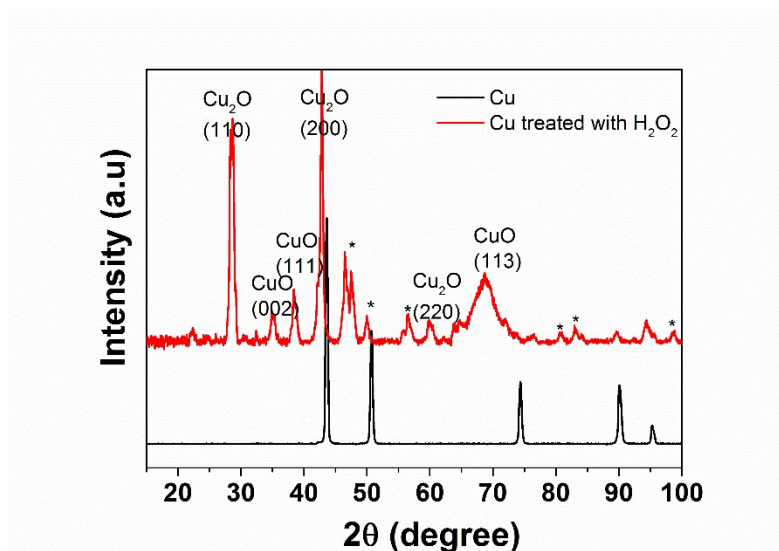
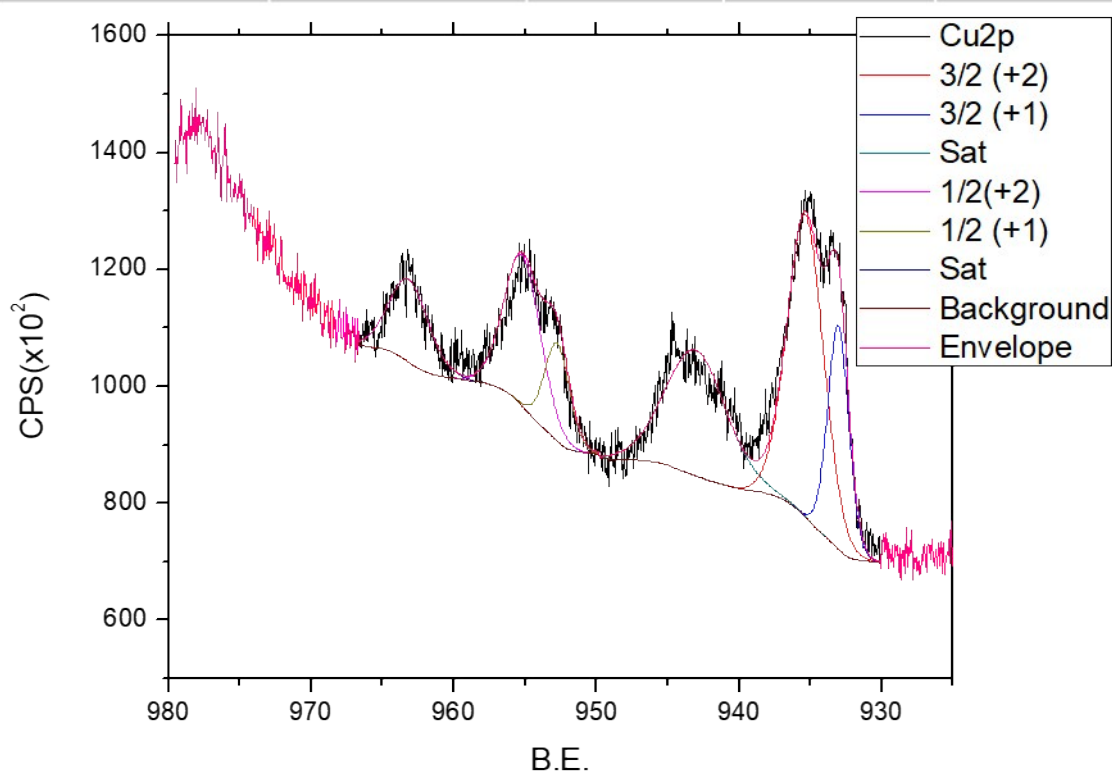


**Fig. S6** XRD patterns of pure Cu before and after  $\text{H}_2\text{O}_2$  treating indicating mixture composite ( $\text{Cu}_2\text{O}$  and  $\text{CuO}$ )<sup>10,11</sup> formed after  $\text{H}_2\text{O}_2$  treatment. \*represent impurity peaks.

TiO2 Cu W: Cu2p				
Name	Peak Pos. (eV)	FWHM	Area	%Area
2p 3/2 (+2)	935.35	3	1682.9	31.859
2p 3/2 (+1)	933.05	1.727	717.0	13.561
2p 1/2 (+2)	943.05	5	1166.5	22.157
2p 1/2 (+1)	955.18	3	841.4	16.069
Satellite 2p 3/2	952.74	2.028	358.5	6.839
Satellite 2p /2	963.14	3.231	496.5	9.516



%Total Area Cu (+2): 70.37%

%Total Area Cu (+1): 29.63%

**Fig. S7** XPS spectra of the oxidized Cu@TiO<sub>2</sub>.

XPS spectra for the Au@TiO<sub>2</sub> in similar conditions (not included) do not show any indication of oxidation.

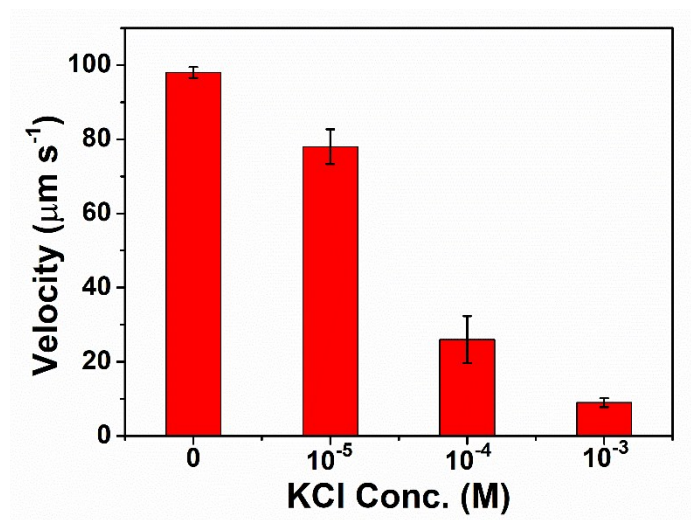


**Fig. S8** dependence of the swimmer velocity on the salt concentration is significantly decreased, which is in line with previous reports on active particles.<sup>12,13</sup>

Videos:

**Video S1** Pure  $\text{TiO}_2$  particles in water with UV light.

**Video S2** Pure  $\text{TiO}_2$  particles in 0.5%  $\text{H}_2\text{O}_2$  with visible light.

**Video S3** Pure  $\text{TiO}_2$  particles in 0.5%  $\text{H}_2\text{O}_2$  with UV light.

**Video S4** Autonomous motion of  $\text{Cu@TiO}_2$  micromotors in water with UV light.

**Video S5** Autonomous motion of  $\text{Cu@TiO}_2$  micromotors in 0.5%  $\text{H}_2\text{O}_2$  with visible light.

**Video S6** Autonomous motion of  $\text{Cu@TiO}_2$  micromotors in 0.5%  $\text{H}_2\text{O}_2$  with UV light.

**Video S7** Active-passive interactions of  $\text{Cu@TiO}_2$  and  $\text{Au@TiO}_2$  micromotors with  $\text{SiO}_2$  particles in water with UV light.

**Video S8** Active-passive interactions of  $\text{Cu@TiO}_2$  micromotors with  $\text{SiO}_2$  particles in 0.5%  $\text{H}_2\text{O}_2$  with visible light.

**Video S9** Active-passive interactions of  $\text{Cu@TiO}_2$  micromotors and  $\text{Au@TiO}_2$  micromotors with  $\text{SiO}_2$  particles in 0.5%  $\text{H}_2\text{O}_2$  with UV light.

All videos (S1-S9) are recorded with 40 frames per second. Video S1-S6 are played with 40 frames per second, and S7-S9 are played with 4X speed (160 fps).

- 1 S. Tanaka, D. Nogami, N. Tsuda and Y. Miyake, *J. Colloid Interface Sci.*, 2009, **334**, 188–194.
- 2 R. Abe, K. Sayama, K. Domen and H. Arakawa, *Chem. Phys. Lett.*, 2001, **344**, 339–344.
- 3 Y. Kakuma, A. Y. Nosaka and Y. Nosaka, *Phys. Chem. Chem. Phys.*, 2015, **17**, 18691–18698.
- 4 J. Zhang and Y. Nosaka, *J. Phys. Chem. C*, 2014, **118**, 10824–10832.
- 5 B. Choudhury and A. Choudhury, *Phys. E Low-dimensional Syst. Nanostructures*, 2014, **56**, 364–371.
- 6 H. Xu, G. Li, G. Zhu, K. Zhu and S. Jin, *Catal. Commun.*, 2015, **62**, 52–56.
- 7 R. Golestanian, T. B. Liverpool and A. Ajdari, *Phys. Rev. Lett.*, 2005, **94**, 1–4.
- 8 W. E. Usual, M. N. Popescu, S. Dietrich and M. Tasinkevych, *Soft Matter*, 2015, **11**, 434–438.
- 9 A. Domínguez, P. Magaretti, M. N. Popescu and S. Dietrich, *Phys. Rev. Lett.*, , DOI:10.1103/PhysRevLett.116.078301.
- 10 J. Chen, B. J. Hansen and G. Lu, *J. Nanomater.*, , DOI:10.1155/2008/830474.
- 11 A. Othonos and M. Zervos, *Nanoscale Res. Lett.*, 2011, **6**, 1–5.
- 12 S. Ebbens, D. A. Gregory, G. Dunderdale, J. R. Howse, Y. Ibrahim, T. B. Liverpool and R. Golestanian, *Europhys. Lett.*, 2014, **106**, 58003.
- 13 A. Brown and W. Poon, *Soft Matter*, 2014, **10**, 4016–4027.